HHS Public Access

Author manuscript

Mol Cell. Author manuscript; available in PMC 2018 December 07.

Published in final edited form as:

Mol Cell. 2017 December 07; 68(5): 993–1005.e9. doi:10.1016/j.molcel.2017.10.019.

Base-resolution mapping reveals distinct m^{1}A methylome in nuclear- and mitochondrial-encoded transcripts

Xiaoyu Li[1,#], **Xushen Xiong**[1,2,3,#], **Meiling Zhang**[1,#], **Kun Wang**[1,#], **Ying Chen**[4,#], **Jun Zhou**[5], **Yuanhui Mao**[5], **Jia Lv**[6], **Danyang Yi**[1], **Xiao-Wei Chen**[3,6], **Chu Wang**[3,4], **Shu-Bing Qian**[5], and **Chengqi Yi**[1,2,4,*]

[1]State Key Laboratory of Protein and Plant Gene Research, School of Life Sciences, Peking University, Beijing 100871, China

[2]Academy for Advanced Interdisciplinary Studies, Peking University, Beijing 100871, PR China

[3]Peking-Tsinghua Center for Life Sciences, Peking University, Beijing, China

[4]Department of Chemical Biology and Synthetic and Functional Biomolecules Center, College of Chemistry and Molecular Engineering, Peking University, Beijing 100871, China

[5]Division of Nutritional Sciences, Cornell University, Ithaca, New York 14853, USA

[6]Institute of Molecular Medicine, Peking University, Beijing, China

SUMMARY

Gene expression can be post-transcriptionally regulated via dynamic and reversible RNA modifications. N^1-methyladenosine (m^{1}A) is a recently identified mRNA modification; however, little is known about its precise location and biogenesis. Here, we develop a base-resolution m^{1}A profiling method, based on m^{1}A-induced misincorporation during reverse transcription, and report distinct classes of m^{1}A methylome in the human transcriptome. m^{1}A in 5′-UTR, particularly those at the mRNA cap, associate with increased translation efficiency. A different, small subset of m^{1}A exhibit a GUUCRA tRNA-like motif, are evenly distributed in the transcriptome and are dependent on the methyltransferase TRMT6/61A. Additionally, we show that m^{1}A is prevalent in the mitochondrial-encoded transcripts. Manipulation of m^{1}A level via TRMT61B, a mitochondria-localizing m^{1}A methyltransferase, demonstrates that m^{1}A in mitochondrial mRNA interferes with translation. Collectively, our approaches reveal distinct classes of m^{1}A methylome and provide a resource for functional studies of m^{1}A-mediated epitranscriptomic regulation.

*Correspondence and Lead Contact: chengqi.yi@pku.edu.cn (C. Y.).
#These authors contributed equally to this work.

AUTHOR CONTRIBUTIONS

X.L., X.X., and C.Y. conceived the base-resolution method and performed sequencing; Y.C., M.Z., K.W., J.L., and D.Y. performed MS analysis and cell biology experiments, under the guidance of C.Y., C.W., and X.-W.C. X.L., K.W., and J.Z. performed ribosome profiling and translation experiments. X.X. designed and performed the bioinformatics analysis, with the help of Y.M. C.Y. and S.-B.Q. supervised the project. All authors commented on and approved the paper.

eTOC blurb

Li et al. developed a single-nucleotide-resolution technology, named "m^1A-MAP", to profile m^1A in the human transcriptome, and revealed distinct classes of m^1A methylome in nuclear- and mitochondrial-encoded transcripts.

INTRODUCTION

More than 100 different types of post-transcriptional modifications have been identified so far (Machnicka et al., 2013). Recent breakthroughs in sequencing technologies have greatly advanced our understanding to the location, regulation, and function of RNA modifications in the transcriptome (Frye et al., 2016; Fu et al., 2014; Helm and Motorin, 2017; Li et al., 2016b), leading to the emerging field of epitranscriptomics (He, 2010; Saletore et al., 2012). One such example is N^1-methyladenosine (m^1A), a prevalent modification in non-coding RNA (ncRNA) and messenger RNA (mRNA) (Anderson and Droogmans, 2005; Dominissini et al., 2016; Li et al., 2016a; Roundtree et al., 2017). m^1A was first documented more than 50 years ago (Dunn, 1961); later it was found to be a primordial RNA modification across the three major phylogenetic domains (Machnicka et al., 2013). In human cells, m^1A is found at position 9 and 58 of human mitochondrial and cytoplasmic tRNAs, catalyzed by TRMT10C, TRMT61B and TRMT6/61A, respectively (Chujo and Suzuki, 2012; Ozanick et al., 2005; Vilardo et al., 2012); it is also present at position 1322 of 28S rRNA, catalyzed by NML (Waku et al., 2016). Its unique physicochemical property has also endowed m^1A with pivotal roles in maintaining the proper structure and function of these ncRNAs (Roundtree et al., 2017). m^1A in tRNA has also been systematically evaluated by microarray and sequencing (Cozen et al., 2015; Saikia et al., 2010; Zheng et al., 2015); more recently, m^1A58 is shown to be reversible by ALKBH1, demonstrating an example of reversible tRNA modification in translation regulation (Liu et al., 2016). In addition to ncRNAs, m^1A is also found to be a dynamic modification in mammalian mRNA, with strong enrichment in the 5′-UTR (Dominissini et al., 2016; Li et al., 2016a).

Despite such rapid progress, a high-resolution profile of the mammalian m^1A methylome is still lacking, significantly limiting our understanding and functional characterization of this newly discovered mRNA modification. Previous m^1A profiling technologies have a resolution of about tens of nucleotides to several hundred nucleotides, primarily determined by the size of RNA fragments in these experiments (Dominissini et al., 2016; Li et al., 2016a). In addition, the methyltransferase(s) and functional consequence of mRNA m^1A modification is poorly understood. Hence, except for a handful positions in rRNA and tRNA, little is known about the precise location, regulation and function of m^1A in the human transcriptome.

Here, we report a base-resolution method to profile m^1A in the human transcriptome. Our method is based on m^1A-induced misincorporation during reverse transcription and reveals distinct classes of m^1A methylome: a major group of m^1A sites that are enriched in 5′-UTR, a small subset of GUUCRA("R" denotes a purine)-tRNA like m^1A sites with relatively even distribution in the transcriptome, and prevalent m^1A modification in the CDS of 10/13 mitochondrial(mt)-encoded transcripts. m^1A sites in the 5′-UTR, particularly those located

at the first and second nucleotide of mRNA transcripts (or “cap+1” and “cap+2” position), are associated with increased translation efficiency. In contrast, m^1A in the CDS of mt-mRNA inhibits translation. Collectively, our approaches reveal distinct classes of base-resolution m^1A methylome in the nuclear- and mitochondrial-encoded transcripts, and provide an in-depth resource towards elucidating the functions of m^1A methylation in mRNA.

DESIGN

Because m^1A can cause both truncation and misincorporation during cDNA synthesis (Hauenschild et al., 2015; Zubradt et al., 2017), we first established the truncation and mutation profiles of different reserve transcriptases (RTases). We systematically compared the performance of several commercially available RTases (including AMV, SuperScript II, SuperScript III and TGIRT) under different conditions (Figure S1). We found that m^1A can precisely induce misincorporation at the site of modification, while m^1A-induced truncation is less accurate and can occur to the neighboring nucleotides. In addition, the truncation profile could be complicated by RNA secondary structures and the fragmentation process needed for library preparation. We concluded that the mutation profile contains a higher signal/noise ratio and is more precise in detecting the exact position of m^1A. Among the RTases we tested, TGIRT demonstrated excellent read-through efficiency and relatively high mutation frequency at the site of m^1A (Figure S1B), consistent with the recent DMS-MaPseq and DM-tRNA-seq results (Zheng et al., 2015; Zubradt et al., 2017). Moreover, we employed a ligation-based strand-specific library preparation protocol (Van Nostrand et al., 2016), which ensures that the m^1A-induced mutation is within the sequenced fragment (see Method Details).

Because we only observed ~40–50% mutation rate at m^1A1322 in 28S rRNA (Figure S2A), which is known to be of high modification level, we further examined the quantitative capability of TGIRT. We chemically synthesized two model RNA sequences with site-specific m^1A modification. For m^1A sites with ~97–98% modification level (measured by quantitative mass spectrometry) (Figure S2B), we consistently observed ~66–75% misincorporation (Figure S2C); the mismatch rate dropped non-linearly when we gradually lowered the modification level. Even with ~50% m^1A modification, a mismatch rate of only ~9–10% was observed (Figure S2C). These findings suggest that the observed mutation rate is an underestimation of the actual modification level. While the TGIRT-based procedure can still detect m^1A sites of high modification level, sequencing RNA directly with TGIRT may not be able to capture the m^1A sites with averaging modification level in the transcriptome (~20% as previously measured by microarray) (Dominissini et al., 2016). To improve the sensitivity for transcriptome-wide m^1A detection, we decided to couple the TGIRT-based procedure with an antibody mediated pre-enrichment step and an additional *in vitro* demethylation step (Figure 1A). We first showed that *in vitro* demethylation reaction mediated by the demethylase AlkB is more efficient than the Dimroth reaction, demonstrating ~98% and ~80% efficiency (Figure S2D), respectively. In addition, the extended treatment of RNA in alkaline condition during the Dimroth reaction leads to excessive RNA degradation (Figure S2E), potentially causing loss of RNA molecules. By integrating the enrichment and demethylation steps, we successfully maximized the dynamic

range of m^1A-induced mutational signature for m^1A1322 in 28S rRNA (~47%, ~95% and ~0.9% in the Input, (−) and (+) demethylase samples, respectively), allowing sensitive and confident m^1A detection (Figure 1B). We termed our approach misincorporation-assisted profiling of m^1A, or m^1A-MAP.

RESULTS

m^1A-MAP detects m^1A in tRNA

We first applied m^1A-MAP to tRNA. In mammals, m^1A can occur at position 9, 14 and 58 of tRNA (Anderson and Droogmans, 2005). m^1A14 has been reported only in $tRNA^{Phe}$ and is considered to be very rare (Machnicka et al., 2013); we did not observe any m^1A modification at position 14 for cytosolic tRNAs in HEK293T cells (Table S1). m^1A58 is conserved across the three domains of life; previous tRNA microarray and sequencing data has reported hypomodified tRNAs at this position (Cozen et al., 2015; Saikia et al., 2010; Zheng et al., 2015). Our results confirmed that m^1A58 is globally present in the cytosolic tRNAs (Figure 1C and S2F). A recent study reported m^1A at position 9 in cytosolic $tRNA^{Asp(GUC)}$ (Clark et al., 2016); this site is also detected by m^1A-MAP (Figure 1D). Collectively, these observations suggest that m^1A-MAP is highly sensitive in detecting m^1A at single-base resolution.

Single-nucleotide resolution m^1A methylome in the transcriptome

We then sought to detect transcriptome-wide m^1A methylome at single-base resolution. We defined two parameters to evaluate the m^1A-MAP data: difference of mismatch rate and fold change of mismatch rate (see Method Details). To minimize the effect of mismatch rate variation during m^1A identification, we rigorously tested our threshold and identified 740 m^1A sites in the 293T transcriptome (Table S1–3). To evaluate potential false positives caused by m^1A-independent mismatch, we performed a “reverse calculation” in which we artificially took the mismatch rate in (−) demethylase as the background and (+) demethylase as the signal, and retrieved only 17 such sites (see Method Details). Moreover, we also systematically evaluated the mutation pattern of the identified m^1A sites in the transcriptome. Using m^1A sites in tRNA as positive controls, we found that m^1A-induced mutation is more strongly influenced by its 5′-nucleotide than the 3′-nucleotide; importantly, a similar sequence-dependent feature is also observed for m^1A sites in mRNA (Figure 2A and S3A). Therefore, we conclude that our strict threshold allowed us to confidently detect transcriptome-wide m^1A sites at single-nucleotide resolution.

Out of the 740 m^1A modifications in the transcriptome (Figure S3B), 473 sites are located in mRNA and lncRNA molecules (Figure S3C and Table S2). Majority of these sites are within the 5′-UTR (Figure 2B and 2C), consistent with the previous finding (Dominissini et al., 2016; Li et al., 2016a). Our single-base profile also reveals multiple features of the m^1A methylome: for instance, we found 24 m^1A methylation sites that are present exactly at the first nucleotide of the 5′ end of the transcripts (Figure 2D and Table S2). Out of the 24 cap +1 m^1A methylation, 22 are found in mRNA while the other 2 are located in lncRNA (Table S2). We further validated these cap+1 m^1A sites using an antibody-independent, locus-specific approach (Figure S3D). We also found 3 additional transcripts with m^1A

methylation at the second nucleotide. For m^1A located in CDS, while we did not observe a tendency for codon position, we did notice a mild preference for codon types, with Arg(CGA) being the most frequently modified by m^1A (Figure S3E). No m^1A is detected for AUG start codons. Representative examples of m^1A sites identified from different mRNA regions are shown (Figure 2D–F and S3F). Two additional sites of high mutation, which are insensitive to the demethylase treatment, also appeared in the *WDR18* and *BRD2* examples (Figure 2D and 2E). By referring to the SNP database, we found that these two positions belong to annotated SNP sites, demonstrating the robustness of our approach in distinguishing true m^1A sites from false signals (SNP, other modifications and etc.).

Because m^1A is enriched in the 5′-UTR, we examined whether m^1A could be involved in translation regulation. We performed ribosome profiling and compared the translation efficiency for transcripts with or without m^1A. We found that m^1A within the 5′-UTR positively correlates with the translation efficiency of mRNA (Figure 2G), in agreement with a previous report (Dominissini et al., 2016). This positive correlation is even stronger for m^1A at the cap+1 position, but is not observed for m^1A located in CDS nor 3′-UTR. This observation hints that m^1A within different regions of mRNA may have different biological functions.

A subset of m^1A sites demonstrate a GUUCRA consensus motif

An unbiased motif detection using DREME revealed that a subset of m^1A (53 sites) are found within a strong GUUCRA sequence (Figure 3A). Interestingly, these sites demonstrate a very different distribution pattern: instead of being enriched in the 5′-UTR, these sites are evenly distributed in the transcriptome (Figure 3B). Because this motif is reminiscent of the m^1A-containing TψC loop in tRNA, we hypothesized that the tRNA methyltransferase complex TRMT6/61A could be responsible for these mRNA m^1A sites. We first performed direct m^1A sequencing (without antibody enrichment) to RNA population below 200 nt to examine the substrate specificity of TRMT6/61A. We found that the m^1A58 sites within the GUUCRA motif experienced a global decrease of mutation rate in the TRMT6/61A knock-down sample, which was not observed for m^1A58 sites that do not confine to the motif (Figure 3C, S4A and S4B). This result suggests that TRMT6/61A-mediated m^1A methylation is highly sequence-specific, consistent with evidence from crystal structures (Finer-Moore et al., 2015). We then analyzed the secondary structure for the 53 mRNA m^1A sites, and found highly conserved structural features compared to the T-loop of tRNA (Figure S4C and S4D). We also picked 3 m^1A sites (in CDS, 3′-UTR and lncRNA, respectively) and examined their response after TRMT6/61A knock-down using a locus-specific approach (Figure 3D). This approach is based on targeted amplification using specific primers (see Method Details), hence enabling us to interrogate these sites with high sequencing depth. The results unambiguously demonstrated a decrease in the mismatch rate for these 3 sites after TRMT6/61A knock-down (Figure 3D). As a comparison, a non-motif m^1A site located in a different structural context demonstrated an unaltered modification status (Figure 3E). Taken together, these observations suggest that in addition to tRNA, TRMT6/61A is also responsible for a subset of m^1A sites in mRNA.

Distinct m^{1}A methylome in the mitochondrial transcriptome

In addition to the nuclear-encoded transcripts, we also detected prevalent m^{1}A modification in the mitochondrial (mt) transcriptome. mt-tRNAs are known to contain m^{1}A at position 9 and 58 (Suzuki et al., 2011), catalyzed by TRMT10C and TRMT61B (Chujo and Suzuki, 2012; Vilardo et al., 2012), respectively. m^{1}A-MAP showed that all the 14 mt-tRNAs bearing an adenosine residue at position 9 are m^{1}A modified; for position 58, m^{1}A was detected for the 3 known and 2 additional mt-tRNA molecules (Figure 4A, 4B and Table S3). For mt-rRNA, the only known m^{1}A site is at position 947 of 16S rRNA (Bar-Yaacov et al., 2016). Interestingly, we additionally detected 7 and 10 m^{1}A sites in 16S and 12S mt-rRNA, respectively (Figure 4 and Table S3). This is very different from cytosolic rRNA, where only one m^{1}A site in 28S rRNA (m^{1}A1322) was found. Unlike m^{1}A947 in 16S mt-rRNA and m^{1}A1322 in 28S rRNA (both are highly modified), the newly detected m^{1}A sites are relatively low in modification level (Table S3). We further validated the presence of m^{1}A in 12S mt-rRNA by both quantitative MS and a primer extension assay (Figure 4C, S5A and S5B).

In human mitochondria, mRNAs are transcribed from the heavy and light strands as polycistronic units (Falkenberg et al., 2007; Mercer et al., 2011). The processed mt-mRNAs lack a cap at the 5′ end and contain no or short untranslated regions (Richter-Dennerlein et al., 2015; Rorbach and Minczuk, 2012; Temperley et al., 2010). We identified 22 m^{1}A sites from 10/13 mitochondrial genes, in which 21 are residing in CDS and 1 is located in the 3′-UTR (Figure 4A and 4B). This is distinct to the m^{1}A methylome in the nuclear-encoded transcripts, where m^{1}A is enriched in the 5′-UTR. In addition, no preference for codon types was observed, yet m^{1}A appears to be more likely present at the third position of a codon in the CDS of mt-mRNA (Figure S5C). By analyzing the published CLASH results in which microRNA and their direct mRNA targets are captured (Helwak et al., 2013), we found two m^{1}A sites that are located within the experimentally verified targets of microRNA (Figure S5D). In fact, these m^{1}A sites reside exactly within mRNA sequences that form base-pairing with the seed regions of microRNAs. More m^{1}A sites in mt-mRNA were found within the predicted mt-mRNA targets of the microRNA seed regions (Figure S5D). Lastly, we also identified 25 m^{1}A sites within the intergenic spacers. 24/25 m^{1}A sites are in the light strand (Figure 4B); some of these m^{1}A sites could be within the 3′-UTR of *MT-ND6*, for which there is no current consensus of its 3′ end (Slomovic et al., 2005).

We further validated m^{1}A1374 in the *MT-ND5* mRNA, and observed a clear band corresponding to m^{1}A1374-induced RT arrest in the Input sample (without immunoprecipitation) using the primer extension assay (Figure 4D). Because the modification level of this site appears to be the highest among the m^{1}A sites in mt-mRNAs (Table S3), we also surveyed publicly available RNA-seq data for the presence of m^{1}A at this position (Kondo et al., 2017; Li et al., 2016a; Li et al., 2015; Quiros et al., 2017). Although the RT conditions differ greatly among the datasets, we were able to consistently find a mutation rate of ~2–9% for this position (Figure 4E). Interestingly, the modification level of m^{1}A1374 appears to be dynamically regulated by different stress conditions (Figure 4E). For instance, its modification level is upregulated under heat shock and hypoxia conditions, while is down-regulated upon serum starvation and actinonin treatment, a drug

that alters mitochondrial proteostasis. Hence, similar to the nuclear genome-encoded mRNA m^1A methylome (Dominissini et al., 2016; Li et al., 2016a), m^1A in mt-mRNA is also dynamically regulated.

m^1A in mt-mRNA interferes with mitochondrial translation

We next sought to examine the biological consequence of m^1A in the mt-mRNAs. Translation requires accurate base pairing between mRNA codons and the cognate tRNAs; however, m^1A is known to block the canonical A:U base pairing. These facts prompted us to hypothesize that m^1A in mt-mRNA, which are primarily located in CDS, could interfere with translation in mitochondria. We first integrated published mitochondria ribosome profiling data with m^1A-MAP identified m^1A methylome in mitochondria (Rooijers et al., 2013). We found a strong signal of mitochondrial ribosome stalling at the m^1A site on *MT-ND5* (Figure 5A and S5E), whose modification level is the highest among all m^1A sites in mt-mRNA. Due to the difficulty of an *in vitro* mitochondrial translation system (Smits et al., 2010), we sought to enzymatically manipulate the modification level of the mt-mRNAs. Two enzymes are known to introduce m^1A in human mitochondria: TRMT10C generates m^1A as well as m^1G at position 9 in mitochondrial tRNAs, while TRMT61B is responsible for m^1A at position 58 in some mitochondrial tRNAs and position 947 in 16S mt-rRNA (Bar-Yaacov et al., 2016; Chujo and Suzuki, 2012; Vilardo et al., 2012). Because TRMT10C is a subunit of the mitochondrial RNase P complex and is not specific for adenosine, we focused on TRMT61B. We utilized sequencing and a qPCR-based assay to quantitatively evaluate the modification status of the m^1A sites in mt-mRNAs (see Method Details). While TRMT61B knock-down mildly reduced the m^1A level (Figure S5F and S5G), TRMT61B overexpression could greatly increase the m^1A modification level (Figure S5F and S5H). More specifically, we found that 5 (*MT-CO1, MT-CO2, MT-CO3, MT-CYB, MT-ND4L*) out of the 10 m^1A-modified mt-mRNAs were targeted by TRMT61B (Figure 5B and Table S4). This observation suggests that in addition to mt-tRNA and mt-rRNA, TRMT61B could also modify mt-mRNA. Because of the high efficiency of TRMT61B overexpression in increasing the m^1A level, we used mass spectrometry to quantitatively measure the mitochondrial protein level upon TRMT61B overexpression (Figure S5I). Indeed, TRMT61B overexpression led to a reduced protein level for MT-CO2 and MT-CO3 (Figure 5C and S5J), which are components of Complex IV; importantly, for *MT-ATP6* and *MT-ATP8* that are not targeted by TRMT61B, their protein levels remain unaffected. We also used metabolic labelling to further demonstrate that TRMT61B overexpression-induced translation repression is specific to mt-mRNA targets of TRMT61B, but not to non-targets of TRMT61B (Figure 5D). We further confirmed this observation using Western blot for MT-CO2 and MT-ATP6, a target and non-target of TRMT61B, respectively (Figure 5E). Of note, upon TRMT61B knock-down, the protein productions for several non-targets of TRMT61B were reduced (Figure S5K), presumably due to the decreased modification level in tRNA and rRNA m^1A sites (which are originally highly modified and beneficial for translation) (Bar-Yaacov et al., 2016; Chujo and Suzuki, 2012). Collectively, these results suggest that m^1A in mt-mRNA interferes with translation in mitochondria.

DISCUSSION

In this study, we developed a single-nucleotide resolution method for transcriptome-wide identification of m^1A in human cells. m^1A-MAP utilizes the m^1A-induced misincorporation in cDNA synthesis to achieve base-resolution m^1A detection. This enabled us to identify m^1A modification not only at the mRNA cap, but also within a GUUCRA tRNA-like sequence motif. In principle, such misincorporation-dependent strategy could be applied to estimate the modification status of RNA sites of interest. However, our results in both rRNA and model RNA sequences strongly suggest that such estimation should be done with caution: TGIRT underestimates m^1A modification level and m^1A-induced mismatch decreases in a non-linear fashion as the modification level decreases. Additionally, the sequence context of RNA has also been reported to affect the mutation rate (Hauenschild et al., 2015; Zubradt et al., 2017). Hence, while direct sequencing (without enrichment) could still detect m^1A sites with high modification level, m^1A sites with averaging modification level or those located within a non-optimal context for mismatch induction could be missed. Therefore, coupling the pre-enrichment step to the mutational signature is necessary to improve the detection sensitivity. In addition, to achieve high confidence, we employed an *in vitro* demethylation step, which enabled us to distinguish true m^1A sites from false signals (SNP, other modifications, and etc.) in the transcriptome. The combined use of mutational signature, the pre-enrichment step and the *in vitro* demethylation step enabled m^1A-MAP to achieve high sensitivity and confidence. Of note, AlkB also demethylates several other methylations in RNA (e.g, m^3C and m^1G) (Cozen et al., 2015; Zheng et al., 2015), hence with the help of specific antibodies for these methylations, our strategy could in principle be applied to these modifications as well.

Our study revealed that two known m^1A modification machinery, TRMT6/61A and TRMT61B, could work on mRNA as well. The hetero complex TRMT6/61A recognizes the sequence and structure of the tRNA T-loop and installs an m^1A at the 58 position (Finer-Moore et al., 2015). Consistent with this knowledge, we found that the TRMT6/61A-dependent mRNA m^1A sites are also confined to a hairpin structure mostly frequently with a 7nt loop, reminiscent of the tRNA T-loop. In contrast, we did not find an obvious sequence context for the m^1A in mt-mRNA. In fact, TRMT61B appears to be a promiscuous enzyme that also modifies mt-tRNA and mt-rRNA; the substrate specificity and the underlying mechanism of TRMT61B in the human mitochondria remains to be determined. In addition, the fact that both TRMT6/61A and TRMT61B are known tRNA modification enzymes also reminds us of the modification machinery for other mRNA modifications. For instance, eukaryotic ψ synthases PUS1, PUS7 and TRUB1 can work on both tRNA and mRNA (Carlile et al., 2014; Li et al., 2015; Lovejoy et al., 2014; Safra et al., 2017; Schwartz et al., 2014a); yet the modification complex for m^6A, consisting at least METTL3, METTL14, WTAP and KIAA1429, appears to be dedicated to mRNA (Bokar et al., 1997; Liu et al., 2014; Ping et al., 2014; Schwartz et al., 2014b). In the case of m^1A, the enzyme(s) responsible for the majority of the modification sites in mRNA remains to be identified. It would be interesting to see if such machinery is specific for mRNA or promiscuous for multiple RNA substrates.

Our base-resolution m^1A profiles reveal distinct m^1A methylome in the human transcriptome. m^1A is enriched in the 5′-UTR; and only 5′-UTR m^1A sites, but not those in CDS nor 3′-UTR, are correlated with higher translation efficiency. Different from the m^1A sites in the nuclear-encoded transcripts, m^1A in mt-mRNA are primarily located in CDS and inhibit translation. Interestingly, m^1A in mt-mRNA can be dynamically regulated, as shown in the case of m^1A in *MT-ND5*. Of note, m^1A517 in *MT-ND2* overlaps with a known site of non-synonymous mutation that is associated with oral cancer (https://www.mitomap.org/MITOMAP). In addition, we also identified a notable group of m^1A methylation adjacent to the mRNA cap; because the first two nucleotides of the 5′ end of mRNA are known to contain ribose methylation, future experiments will be needed to examine whether they are m^1A or m^1A_m modifications. A related but different modification, m^6Am, is also known to be present at this position. Yet, m^6A_m does not induce misincorporation during reverse transcription, nor become sensitive to demethylation by AlkB, as we showed in Figure S3D. Hence, m^1A-MAP is capable of specific detection of methylation at the N1—but not the N6—position of adenosine. Whether the positive association of cap and 5′-UTR m^1A with translation is due to improved mRNA stability (similar to m^6A_m) (Mauer et al., 2017; Schwartz et al., 2014b) or other mechanisms remains to be further studied.

Our results also revealed prevalent m^1A methylation in mt-mRNA; this is due to the utilization of a stranded library preparation strategy in this study as compared to the previous methods (Dominissini et al., 2016; Li et al., 2016a). Similar stranded library preparation strategy has also enabled the identification of pseudouridylation in mt-mRNA (Antonicka et al., 2017). We also showed that such methylation interferes with translation. By manipulating the m^1A level via TRMT61B, we monitored the corresponding changes of the mitochondrial protein level by both quantitative mass spectrometry and Western blot. TRMT61B modifies both mt-tRNA and mt-rRNA (Bar-Yaacov et al., 2016; Chujo and Suzuki, 2012); and these m^1A sites are thought to be beneficial for their functions in translation. Because m^1A sites in mt-mRNA have an opposing effect in translation, changes of protein synthesis level after TRMT61B knock-down could be a mixed result of contrary m^1A sites in these different components (rRNA, tRNA and mRNA) of translation. Conversely, because16S rRNA and mt-$tRNA^{Leu(UUR)}$ are already of high m^1A level, we envisioned that TRMT61B overexpression should lead to a greater increase of m^1A level in mRNA than in these ncRNAs. In this simplified scenario, we indeed observed greatly increased modification level for several mt-mRNAs upon TRMT61B overexpression and detected reduced protein level for such mt-mRNA transcripts. Importantly, protein levels for non-targets of TRMT61B, which are either devoid of m^1A or contain TRMT61B-independent m^1A sites, remain unaffected upon TRMT61B overexpression. Hence, TRMT61B overexpression-mediated translation repression is caused by mt-mRNA m^1A and is specific to its mt-mRNA targets. For the mt-mRNAs that contain TRMT61B-independent m^1A sites, additional methyltransferase(s), for instance TRMT10C that is also localized in the mitochondrial, may be involved. In terms of the mechanism of m^1A-mediated translational suppression, multiple possibilities need to be considered. For instance, due to the presence of a base-pairing interfering modification in the CDS, m^1A could serve as a road block for the mitochondrial ribosome. In fact, recent *in vitro* translation experiments on synthetic RNA sequences have shown that m^1A in CDS represses translation; the effect is

stronger when m^1A is at codon position 1 and 2, while m^1A at the third position also mitigates translation (You et al., 2017). Thus, not only the stoichiometry but also the exact position of m^1A in mt-mRNA could influence protein synthesis. In addition, we showed that the presence of m^1A in mt-mRNA could interfere with base pairing to microRNA, which is thought to enhance translation in mitochondria (Zhang et al., 2014). While both the speculated mechanisms point to a suppressive role of m^1A in mitochondria translation, alternative hypothesis and mechanism should also be tested in future experiments. Nevertheless, our discovery that m^1A in mt-mRNA interferes with translation improves our understanding of translation regulation in human mitochondria.

In summary, our study demonstrated distinct classes of m^1A methylome in the nuclear- and mitochondrial-encoded transcripts. Our single-nucleotide resolution m^1A technology allowed the comprehensive profiling of m^1A in the human transcriptome, providing a reference and resource for future investigations to elucidate the biological functions and mechanisms of this epitranscriptomic mark.

Limitations

Our current procedure of m^1A-MAP favors sensitivity and accuracy over the quantitative ability, due to the involvement of a pre-enrichment step using an m^1A antibody. For the m^1A sites located in abundant RNAs (rRNA, tRNA and a limited subset of mRNA), their modification levels could be estimated by comparing the mismatch rates in the Input sample with a stoichiometry curve (similar to Figure S2C). However, for the majority of mRNA molecules in the transcriptome, only limited sequencing reads could be obtained by transcriptome-wide sequencing experiments. Thus, stoichiometry for m^1A sites in less abundant mRNA molecules may not be reliably estimated by their mismatch rates in the Input sample. To address this limitation, the modification level of m^1A-MAP identified m^1A sites can be estimated via additional locus-specific sequencing to the Input samples, which would allow sufficient sequencing depth while remain cost-effective. The exact stoichiometry of these sites can then be determined by fitting the mismatch rates in the locus-specific sequencing into the stoichiometry curve of synthetic spike-in RNAs that contain the exact sequence of the RNA molecules of interest.

STAR METHODS

CONTACT FOR REAGENT AND RESOURCE SHARING

Further information and requests may be directed to, and will be fulfilled by the corresponding author Chengqi Yi (chengqi.yi@pku.edu.cn).

EXPERIMENTAL MODEL AND SUBJECT DETAILS

HEK293T was maintained at 37 °C in DMEM medium (Gibco) supplemented with 10% FBS (Gibco) and 1% penicillin/streptomycin (Gibco).

METHOD DETAILS

Cell Culture and Antibodies—HEK293T (ATCC, CRL-11268) was used in this study and maintained in DMEM medium (Gibco) supplemented with 10% FBS (Gibco) and 1%

penicillin/streptomycin (Gibco). Monoclonal mouse anti-m^1A antibody was purchased from MBL (D345-3). Polyclonal rabbit anti-TRMT6 antibody was purchased from Santa Cruz Biotechnology (sc-271752). MT-CO2 antibody (55070-1-AP) and MT-ATP6 antibody (55313-1-AP) was purchased from Proteintech Group. Monoclonal mouse anti-β-Actin antibody was purchased from CWBiotech (CW0096). Monoclonal mouse anti-GAPDH antibody was purchased from CWBiotech (CW0100M). The secondary antibodies used were anti-mouse-IgG-HRP (CW0102; CWBiotech) and anti-rabbit-IgG-HRP (CW0103; CWBiotech).

RNA isolation—Total RNA was isolated from cells using TRIzol, according to the manufacturer's instructions (Invitrogen). An additional DNase I treatment step was performed to avoid DNA contamination. For $polyA^+$ RNA isolation, small RNA was firstly depleted using MEGAclear™ Transcription Clean-Up Kit (Ambion), followed by two successive rounds of $polyA^+$ selection using $oligo(dT)_{25}$ Dynabeads (Invitrogen). For small RNA isolation, RNA smaller than 200 nt was recovered from the flow-through fraction in the small RNA depletion step by ethanol precipitation.

shRNA knock-down of TRMT6/61A—The oligoes targeting TRMT6 and TRMT61A were annealed and cloned into the pLKO vector according to the TRC shRNA library protocol (http://www.broadinstitute.org/rnai/public/), respectively. The oligo sequences were listed below: TRMT6-FWD: CCGGGGGAAAGTTCTGAGTATTTATCTCGAGATAAATACTCAGAACTTTCCCTTTTTG; TRMT6-RVS: AATTCAAAAAGGGAAAGTTCTGAGTATTTATCTCGAGATAAATACTCAGAACTTTCCC; TRMT61A-FWD: CCGGGAGGCCAGAGGCACCTTATATCTCGAGATATAAGGTGCCTCTGGCCTCTTTTTG; TRMT61A-RVS: AATTCAAAAAGAGGCCAGAGGCACCTTATATCTCGAGATATAAGGTGCCTCTGGCCTC. A scrambled shRNA was used as the mock control. Lentiviruses were packaged by co-transfecting HEK293T cells with pLKO-TRMT6, pLKO-TRMT61A, pCMV-dR8.91 and VSV-G plasmids, following the instructions from Broad Institute. The supernatant from transfected cells was harvested after 2 days and used to infect HEK293T cells followed by puromycin selection for 5 days. Knock-down efficiency was verified by Western blot and qPCR. qPCR primers were listed as follows: TRMT6-qFWD: CTGTCTTTGCTGGACTTTGTGGC; TRMT6-qRVS: AGACAGCCTGAGGTTGATGACC; TRMT61A-qFWD: TCCTCTACTCCACAGACATCGC; TRMT61A-qRVS: CAATGGTGCGGATGATGGCGTG.

Quantification of m^1A and m^6A level by LC-MS/MS—200 ng isolated RNA or 100 ng model RNA oligo was digested into nucleosides by 0.5 U nuclease P1 (Sigma, N8630) in 20 μL buffer containing 10 mM ammonium acetate, pH 5.3 at 42 °C for 6 h, followed by the addition of 2.5 μL 0.5 M MES buffer, pH 6.5 and 0.5 U alkaline phosphatase (Sigma, P4252). The mixture was incubated at 37 °C for another 6 h and diluted to 50 μL. 5 μL of the solution was injected into LC-MS/MS. The nucleosides were separated by ultra-

performance liquid chromatography with a C18 column, and then detected by triple-quadrupole mass spectrometer (AB SCIEX QTRAP 5500) in the positive ion multiple reaction-monitoring (MRM) mode. The mass transitions of m/z 282.0 to 150.1 (m^1A), m/z 282.0 to 150.1 (m^6A), m/z 268.0 to 136.0 (A) were monitored and recorded. Concentrations of nucleosides in RNA samples were deduced by fitting the signal intensities into the stand curves.

Stoichiometry curve construction using model oligoes—Two pairs of synthetic RNA oligoes containing either m^1A or A were used to examine the capacity of m^1A in causing mis-incorporation during revers transcription in a quantitative manner. The oligo sequences were listed as follows: m^1A-1: CGCGGCUCG$\underline{m^1A}$GCCCGCGUGCGGGCCUCUUUCAGGCCGCU; A-1: CGCGGCUCG$\underline{A}$GCCCGCGUGCGGGCCUCUUUCAGGCCGCU; m^1A-2: CGGCGGCCCGGGACCG$\underline{m^1A}$GACCCGGCCCCGGCUCCCC; A-2: CGGCGGCCCGGGACCG$\underline{A}$GACCCGGCCCCGGCUCCCC. The m^6A contamination in the m^1A oligoes, which was introduced during the oligo purification process, was measured using quantitative LC-MS/MS. The m^1A-oligo was mixed with the A-oligo to ratios: 100%, 75%, 50%, 25%, 12.5%, 6.25% and 0%, respectively. The mixed m^1A/A oligoes were subjected to library construction using specific RT primers as listed below:

RT-m^1A/A-1: ACACGACGCTCTTCCGATCTagcggcctgaaagaggc;

RT-m^1A/A-2: ACACGACGCTCTTCCGATCTggggagccggggcc.

Cloning, Expression and Purification of AlkB—A truncated AlkB with deletion of the N-terminal 11 amino acids was cloned into pET30a (Novagen) and transformed to E. coli BL21(DE3) followed by culturing in LB medium at 37 °C until the OD_{600} reached 0.6–0.8, and further incubating at 30 °C for additional 4 h with the addition of 1 mM IPTG. Proteins were purified using Ni-NTA chromatography (GE Healthcare) and gel-filtration chromatography (Superdex 200, GE Healthcare) followed by Mono-Q anion exchange chromatography (GE Healthcare). Such purification procedure effectively avoided RNA contamination from *E coli.* (the expression host).

***In vitro* Demethylation treatment—**We employed two different strategies for the removal of methyl-group at the N1 position of adenosine.

In vitro demethylation mediated by the purified AlkB protein: 10 μg full length $polyA^+$ RNA was fragmented at 94 °C for 5 min using magnesium RNA fragmentation buffer (NEB) and fragmented $polyA^+$ RNA was desalted and concentrated by ethanol precipitation. 10 μg (~0.2 nmol) fragmented $polyA^+$ RNA was denatured at 65 °C for 5 min, and then subjected to demethylation reaction in a 500 μL demethylation mixture containing 0.4 nmol purified AlkB, 50 mM MES, pH 6.5, 283 μM of $(NH_4)_2Fe(SO_4)_2{\cdot}6H_2O$, 300 μM 2-ketoglutarate, 2 mM L-ascorbic acid, 1 U/μL SUPERaseIn RNase Inhibitor (Invitrogen). The demethylation reaction was incubated at 37 °C for 2 h and quenched by adding 5 mM EDTA. The demethylated RNA was then purified by phenol chloroform extraction.

In vitro demethylation mediated by the Dimroth rearrangement: 10 μg full length polyA$^+$ RNA was incubated in alkaline buffer (0.1 M Na_2CO_3/$NaHCO_3$, 5mM EDTA, pH 10.2) at 65 °C for 3 h, and then the treated RNA was purified by ethanol precipitation.

m^{1}A-MAP—40 μg polyA$^+$ RNA was fragmented to ~150 nt using magnesium RNA fragmentation buffer (NEB). m^{1}A-containing RNA fragments were enriched through m^{1}A immunoprecipitation as previous described (Li et al., 2016a). 10 ng (~0.2 pmol) of the immunoprecipitated m^{1}A-containing RNA fragments were subjected to the AlkB demethylation treatment. Demethylation reaction was performed in a 20 μL demethylation mixture containing 0.4 pmol purified AlkB, 50 mM MES, pH 6.5, 283 μM of $(NH_4)_2Fe(SO_4)_2{\cdot}6H_2O$, 300 μM 2-ketoglutarate, 2 mM L-ascorbic acid and 0.4 U/μL RNase inhibitor, following with an incubation at 37 °C for 2 h. The reaction was quenched by the addition of 5 mM EDTA, and the demethylated RNA was purified by phenol chloroform extraction followed with ethanol precipitation.

Fragmented polyA$^+$ RNA (as “Input”), immunoprecipitated RNA [as “(−) demethylase”] and demethylated immunoprecipitated RNA [as “(+) demethylase”] were subjected to library construction. The library construction was performed according to the eCLIP library construction protocol with several modifications (Van Nostrand et al., 2016). For dephosphorylation of 3′ ends, RNA samples were treated by PNK (NEB) with an incubation at 37 °C for 1 h, and followed by a heat-inactivation of PNK at 65 °C for 20 min. The dephosphorylated RNA was purified by ethanol precipitation and then subjected to 3′ RNA linker ligation using T4 RNA ligase2, truncated KQ (NEB) at 25 °C for 2 h. The 3′ RNA linker sequence is: 5′rAPP-AGATCGGAAGAGCGTCGTG-3SpC3. The excess RNA adaptor was digested by adding 1 μL 5′ Deadenylase (NEB) into the ligation mix followed by an incubation at 30 °C for 1 h, and then adding 1 μL RecJf (NEB), incubating at 37 °C for another 1 h. The enzymes were then heat-inactivated at 70 °C for 20 min, and the RNA was purified by ethanol precipitation. The RNA pellet was dissolved in 10 μL H_2O and then 1 μL 2 μM RT primer (ACACGACGCTCTTCCGATCT) was added. RNA-primer mix was denatured at 80 °C for 2 min and then chilled on ice immediately. RT reaction buffer (50 mM Tri–HCl pH 8.3, 75 mM KCl, and 3 mM $MgCl_2$, final), dNTPs (1 mM, final), DTT(5 mM, final), RNase Inhibitor (1 U/μL, final) and 1 μL TGIRT (InGex) were added into the denatured RNA-primer mix and reverse transcription was carried out at 57 °C for 2 h. Excess RT primer was digested by the addition of 1 μL Exonuclease I (NEB) and a following incubation at 37 °C for 30 min. cDNA was purified using silane be ads (Invitrogen) and then ligated to the 5′ adaptor (5Phos-NNNNNNNNNNAGATCGGAAGAGCACACGTCTG-3SpC3). Ligation was performed with T4 RNA ligase 1, high concentration (NEB) at 25 °C overnight. The ligated cDNA was purified using silane beads, and then subjected to PCR amplification with the following primers: 5′-AATGATACGGCGACCACCGAGATCTACACTCTTTCCCTACACGAC GCTCTTCCGATCT-3′, 5′-CAAGCAGAAGACGGCATACGAGATXXXXXXGTGACTGGAGTTCAGACGTGTGCT CTTCC GATC-3′ (XXXXXX represents index sequence). PCR product was purified by 8% TBE gel. The libraries were sequenced on Illumina Hiseq X10 with paired-end 2×150 bp read length.

Locus-specific m^1A detection—We developed two different strategies for locus-specific detection of m^1A sites at the first nucleotide of mRNA transcripts and those located internally, respectively.

For cap+1 m^1A detection, 2 μg $polyA^+$ RNA was fragmented to ~150 nt and then equally divided into two parts. One part of RNA sample was subjected to the AlkB demethylation treatment ["(+) AlkB"] and the other part was untreated ["(−) AlkB"]. Demethylation reaction was performed as described above. (+) AlkB and (−) AlkB sample were ligated to 3′ RNA linker (5′rAPP-AGATCGGAAGAGCGTCGTG-3SpC3) and then reverse transcription was carried out using TGIRT with the same RT condition as that of m^1A-MAP. The 5′ cap-adaptor (5Phos- GTCTCAGCGTCCAGTGTCATC-3SpC3) was ligated to the reverse transcribed cDNAs. The regions harboring m^1A were amplified by PCR using a universal forward primer (5′-GATGACACTGGACGCTGAGAC-3′) and gene specific reverse primers (listed in Table S5). The amplicons from different m^1A-containing regions were mixed together for (+) AlkB and (−) AlkB sample, respectively and then subjected to DNA library construction using NEBNext® Ultra™ II DNA Library Prep Kit for Illumina® (E7645) according to the manufacturer's instructions. Deep sequencing for the libraries was performed on Illumina Hiseq X10 with paired-end 2×150 bp read length. Thus, cap+1 m^1A to be validated can be covered with sufficient reads for the reliable examination of mutation rate.

For internal m^1A detection, 200 ng $polyA^+$ RNA was isolated from TRMT6/61A stable knock-down cells and mock control cells respectively, and then was fragmented to 150 nt using magnesium RNA fragmentation buffer (NEB). Fragmented RNA was ligated to 3′ RNA linker (5′rAPP-AGATCGGAAGAGCGTCGTG-3SpC3) and then reverse transcription was carried out using TGIRT with the same RT condition as that of m^1A-MAP. The regions harboring m^1A were amplified by PCR using specific primers. The amplicons from different m^1A-containing regions were mixed together for each sample, and then subjected to DNA library construction using NEBNext® Ultra™ II DNA Library Prep Kit for Illumina® (E7645) according to the manufacturer's instructions. Deep sequencing for the libraries was performed on Illumina Hiseq X10 with paired-end 2×150 bp read length. Thus, the position of m^1A to be validated can be covered with sufficient reads for the examination of mutation rate. Specific PCR primers are listed below:

NM_025099-m^1A5643-FWD: AAAAAGCTCGGTCCGGGTTC;

NM_025099-m^1A5643-RVS: TTAGCCGCAAAATCACGCTG;

NM_001193375-m^1A978-FWD: ACACCTGTCCAAGCCCTAAT;

NM_001193375-m^1A978-RVS: CTGAGGGGCCCTTATTCCCA;

NR_026951-m^1A659-FWD: ACGTCGGCTCGTTGGTCTAG;

NR_026951-m^1A659-RVS: ACAGTCAAGCCTCCTGCAGC;

NM_001256443-m^1A486-FWD: CAAGGTTCCAGGCGAAGGG;

NM_001256443-m^1A486-RVS: AGCCGGGGTCTCTGTGG.

Purification of Mitochondrial 12S mt-rRNA—Total RNA was isolated from cells using TRIzol, according to the manufacturer's instructions (Invitrogen). An additional DNase I treatment step was performed to avoid DNA contamination. Bring 200 μg DNAse I treated total RNA to volume of 160 μL in nuclease-free water, and then add 1 μL 12S mt-rRNA probe mix (20 μM each). The probe mix contains 4 3′-biotin labeled oligoes that specifically target 12S mt-rRNA and the sequences were listed as follows: 12S-probe-1: GAGCTAATAGAAAGGCTAGGAC; 12S-probe-2: TCTATTGACTTGGGTTAATC; 12S-probe-3: TTATCGATTACAGAACAGGCT; 12S-probe-4: TCTACTCTTAGTTTACTGCTAA. The RNA mixture was heated at 65 °C for 10 min and followed by chilling on the ice. 40 μL 5 × Binding buffer (1.5 M NaCl, 10 mM EDTA, 100 mM Tris, pH 7.4) was added into the RNA mixture and mixed well by pipetting. The RNA mixture was incubated at room temperature for about 30 minutes. 200 μL Streptavidin C1 Dynabeads (Invitrogen) was resuspended in 200 μL Binding Buffer (300 mM NaCl, 2 mM EDTA, 20 mM Tris, pH 7.4) and then added into the RNA mixture. The RNA beads mixture was incubated at room temperature for 40 minutes by gently rotating. The beads was washed with Washing Buffer (30 mM NaCl, 1 mM EDTA, 10 mM Tris, pH 7.4, 1% SDS) at 40 °C for four times. RNA was eluted from beads by adding 200 μL Elution buffer (5 mM EDTA, 10 mM Tris, pH 7.4, 1% SDS) and incubating at 70 °C for 10 minutes. Isolated RNA was recovered by ethanol precipitation and 12S mt-rRNA was further selected using 4% Urea-PAGE. The purity of isolated 12S mt-rRNA was checked using RNA 6000 Pico Chip on an Agilent 2100 Bioanalyzer (Agilent Technologies). The m^1A methylation level of 12S mt-rRNA was analyzed by quantitative LC-MS/MS.

Primer extension—The primer extension was performed as previously reported (Bar-Yaacov et al., 2016; Chujo and Suzuki, 2012) with several modifications.

To detect m^1A1374 in *MT-ND5*, 2 μg mRNA was mixed with 10 fmol 5′ biotin labeled primer (ND5- m^1A1374-primer: CCTGCGAATAGGCTTCC) in a 5 μL solution containing 10 mM Tris, pH 7.5 and 1 mM EDTA. The RNA mixture was then heated at 80 °C for 2 min and slowly cooled to 25 °C over 55 min. The RT mixture (containing 2 μL 5× First-Strand Buffer, 1.5 μL 25 mM $MgCl_2$, 0.5 μL 0.1 M DTT, 0.5 μL Superscript III, 0.25 μL RNase inhibitor, 0.25 μL 1.5 mM ddATP, dTTP, dCTP, and dGTP mix) was then added into the RNA mixture and mixed well. The reverse transcription was carried out at 55 °C for 1 h and then the RNA template was digested with RNase H. The reverse transcribed products were separated by 20% Urea-PAGE and then transferred to Nylon membrane, detected by chemiluminescent nucleic acid detection module (Thermo, 89880).

To detect m^1A378 and m^1A575 in 12S mt-rRNA, 50 ng fragmented total RNA or 20 ng immunoprecipitated RNA was mixed with 5 fmol 5′ biotin labeled primer (12S-m^1A378-primer: TGTGTTCAGATATGTTAAAG; 12S-m^1A575-primer: GAGGTGGTGAGGTTGATCG) and then subjected to reverse transcription as described above. The d/ddNTP mix consisted of dATP, dTTP, dCTP and ddGTP for m^1A378 in 12S mt-rRNA; ddATP, dTTP, dCTP and dGTP for m^1A575 in 12S mt-rRNA. The reverse transcription was carried out at 49 °C for 12S-m $^1A378$ and 55 °C for 12S-m^1A575. The reverse transcribed products were analyzed as described above.

siRNA Knock-down and overexpression of TRMT61B—Two synthesized duplex RNAi oligoes targeting TRMT61B mRNA sequences were used: 5′-GGAUAUCAACCCAGGUGAUTT-3′ and 5′-GCGUGAUUCAUGGAAAUUATT-3′; a scrambled duplex RNAi oligo (5′-UCCUCCGAACGUGUCACGUTT) was used as the mock control. The siRNA oligo was transfected into HEK293T by Lipofectamine RNAiMAX (Invitrogen) according to the manufacturer's instructions, and cells were harvested 48 h later after transfection. Knock-down efficiency was examined by qPCR. qPCR primers were listed as follows:

TRMT61B-qFWD: CAGGAGCAACCGAAGACAT;

TRMT61B-qRVS:ATATACAGCACATACACCACCAT;

For the construction of overexpression plasmid, TRMT61B was cloned into pcDNA3.1 using the following primers: FWD: TCGCGAAACACTATGCTAATGGC; RVS: GTTAAGTTGTGGTTTGACCTTCCTC. The empty pcDNA3.1 vector was used as the mock control. The plasmid was transfected into HEK293T by Lipofectamine 2000 (Invitrogen) according to the manufacturer's instructions and cells were harvested 48 h later after transfection.

Ribosome profiling—2 plates of 15-cm HEK293T cells were grown to 90% confluency; CHX was then added to the medium at a final concentration of 100μg/mL. Cells were treated in the CHX-medium for 7 min before they were harvested and lysed with 1 mL lysis buffer (10 mM Tris-HCl, pH 7.4, 5 mM $MgCl_2$, 100 mM KCl, 1% Triton X-100, 2 mM DTT, 100 μg/mL CHX, 0.5 U/μL RNase inhibitor, 1×complete protease inhibitor). The cell lysates were centrifuged at 15,000g for 15min, and the supernatant was collected and sent for the OD260 measuring. 100 μL lysates were kept as input sample and 1 mL TRIzol was added to purify the RNA. 1 μL Micrococcal Nuclease (NEB) per 25OD was added to the remaining cell lysates and incubated at 25 °C for 20 min. The digested cell lysates were used for performing ribosome foot-printing. The lysates were fractioned on 10/50% w/v sucrose gradients using the SW-40Ti rotor at 27,500rpm for 4h. 80S monosome fraction was collected, followed by the addition of equal volume of extraction buffer (1% SDS, 40 mM EDTA). RNA was isolated by phenol-chloroform extraction. RNA fragments between 28–30 nt were selected using 15% Urea-PAGE. Recovered RNA fragments were subjected to library construction. In brief, RNA samples were dephosphorylated with PNK (NEB) and ligated to 3′ RP linker (5′rAPP-CTGTAGGCACCATCAAT-3SpC3) using T4 RNA ligase2, truncated KQ (NEB). Reverse transcription was carried out using Superscript III (Invitrogen) with RP-RT primer (5Phos-AGATCGGAAGAGCGTCGTGTAGGGAAAGAGTGTAGATCTCGGTGGTCGC-SpC18-C ACTCA-SpC18-TTCAGACGTGTGCTCTTCCGATCTATTGATGGTGCCTACAG). cDNA was circ-ligated with CircLigase II (Epicentre) and then amplified by PCR with primers (5′-AATGATACGGCGACCACCGAGATCTACAC-3′; 5′-CAAGCAGAAGACGGCATACGAGATXXXXXXGTGACTGGAGTTCAGACGTGTGCTCTTCC GATC-3′, XXXXXX represents index sequence). PCR products were purified by 8% TBE gel and sequenced on Illumina Hiseq 2500 with single end reads (50 bp).

qPCR-based m^{1}A level evaluation—20 μg polyA$^+$ RNA was isolated from HEK293T cells with TRMT61B overexpression, knock-down and the corresponding mock controls, respectively. RNA was fragmented into ~150 nt using magnesium RNA fragmentation buffer (NEB) and concentrated by ethanol precipitation. Fragmented RNA (as Input) was denatured and incubated with 2 μg anti-m^{1}A antibody in IPP buffer (150 mM NaCl, 0.1% NP-40, 10 mM Tris, pH 7.4) at 4°C overnight. 20 μL Protein A/G UltraLink Resin (Pierce) was added to the RNA-antibody mixture and incubated at 4°C for additional 3 h. Resins were washed for twice with IPP buffer, once with low salt buffer (75 mM NaCl, 0.1% NP-40, 10 mM Tris, pH 7.4), once with high salt buffer (200 mM NaCl, 0.1% NP-40, 10 mM Tris, pH 7.4) and twice with TEN buffer (10 mM Tris, pH 7.4, 1 mM EDTA, pH 8.0, 0.05% NP-40). m^{1}A-containing RNA was eluted from resins with 3 mg/mL N^1-methyladenosine (Berry&Associates) in IPP buffer and purified by phenol chloroform extraction and ethanol precipitation. Input and immunoprecipitated samples were reverse transcribed into cDNA using Superscript III (Invitrogen) and quantified by qPCR using SYBR GREEN mix (Takara) on Roche Lightcycler 96 real-time PCR system. The m^{1}A-IP/Input ratios of the targeted regions were calculated for the TRMT61B overexpression, knock-down and the corresponding control samples, respectively. The primers used for qPCR were listed below:

MT-CO1-qFWD: CCTATCATCTGTAGGCTCATTC;

MT-CO1-qRVS: GGAGGGTTCTTCTACTATTAGGAC;

MT-CO2-qFWD: ACAGATGCAATTCCCGGACG;

MT-CO2-qRVS: CCACAGATTTCAGAGCATTGACC;

MT-CO3-qFWD: CGCCTGATACTGGCATTTTG;

MT-CO3-qRVS: GACCCTCATCAATAGATGGAGAC;

MT-CYB-qFWD: CAACCCCCTAGGAATCACCTC;

MT-CYB-qRVS: GAGGGCGTCTTTGATTGTGTAG;

16S rRNA-qFWD: ATGAATGGCTCCACGAGGG;

16S rRNA-qRVS: CTTGCTGTGTTATGCCCGC.

Reductive dimethylation labeling—Mitochondrion was isolated from TRMT61B overexpression and mock control HEK293T cells according to the manufacturer's (Thermo Fisher) and lysed with RIPA buffer followed by sonication. The extracted proteins from different samples were quantified with the BCA protein assay kit (Thermo Fisher). Equal amount of proteins from two samples were digested by trypsin on-column in 100 mM TEAB buffer and subjected to reductive dimethylation labeling. 4 μL of 4% (w/w) light or heavy formaldehyde was added to 100 μL of trypsin digested samples prepared from TRMT61B overexpression and mock control HEK293T cells, respectively. In the meantime, 4 μL of 0.6 M sodium cyanoborohydride was added and the samples were incubated at room temperature for 1h. The dimethylation labeling reaction was quenched by the addition of 1% (w/w) ammonia and 5% (w/w) formic acid. Finally, light and heavy labeled peptide samples were mixed, concentrated by vacuum, and analyzed on a Q Exactive mass spectrometer (Thermo Fisher).

LC-MS/MS and data analysis—The peptides were analyzed on a Q Exactive mass spectrometer (Thermo Fisher). Under the positive-ion mode, full-scan mass spectra was acquired over the m/z range from 350 to 1800 using the Orbitrap mass analyzer with mass resolution setting of 70000. MS/MS fragmentation was performed in a data-dependent mode, of which the 20 most intense ions were selected from each full-scan mass spectrum for high-energy collision induced dissociation (HCD) and MS2 analysis. MS2 spectra were acquired with a resolution setting of 17500 using the Orbitrap analyzer. Some other parameters in the centroid format: isolation window, 2.0 m/z units; default charge, 2+; normalized collision energy, 28%; maximum IT, 50 ms; dynamic exclusion, 20.0 s.

LC-MS/MS data was analyzed by ProLuCID (Xu et al., 2015) with static modification of cysteine (+57.0215 Da) and variable oxidation of methionine (+15.9949 Da). The searching results were filtered by DTASelect (Tabb et al., 2002) and peptides were also restricted to fully tryptic with a defined peptide false positive rate of 1%. The ratios of reductive dimethylation were quantified by the CIMAGE software as described before (Weerapana et al., 2010).

Pre-processing of raw sequencing data—A random barcode of 10 nt was included in the adapter that ligates to the 3′ end of cDNA and it cannot be precisely located in Read 1. Hence, only Read 2 data of m^1A-MAP was used for subsequent analyses. Raw sequencing reads produced from m^1A-MAP were firstly subjected to Trim_galore (http://www.bioinformatics.babraham.ac.uk/projects/trim_galore/) for quality control and adaptor trimming. The minimum quality threshold was set to 20, and the minimum length required for reads after trimming was 30 nt. The remaining reads were further processed by removing the first 10 nt random barcode in the 5′ end. As for the ribosome profiling (Ribo-seq) data and the corresponding RNA-seq data, reads with a quality lower than 20 were discarded, and the adapter in 3′ end was trimmed. Processed reads with a length ranging from 25 nt to 35 nt in the ribosome profiling sample were kept for further analysis.

Reads mapping and PCR duplication removing—Processed reads were mapped to human transcriptome or mitochondrial genome using BWA-MEM with default parameters (version 0.7.15-r1140) (Li and Durbin, 2009). Reference transcriptome was prepared based on the Refseq annotation of human (hg19) downloaded from the table browser of UCSC database. The redundant sequences with the same Refseq id were removed. Transfer RNA (tRNA) sequences were also downloaded from UCSC table browser and integrated into the transcriptome. Mitochondrial genome and corresponding annotation were downloaded from NCBI (NC_012920.1). Reads mapping to an identical position of reference were considered as PCR duplications if their 10 nt random barcodes were the same, and only one of these reads was kept. Performances related to the processing of sam/bam file were done with the help of SAMtools (Li et al., 2009) (http://samtools.sourceforge.net/).

Identification of m^1A sites—Mismatch rate of each nucleotide in the reference sequences was calculated for both (−) and (+) demethylase samples. Two parameters were defined to evaluate the dynamic change of mismatch rate in the (−) demethylase and (+) demethylase samples: difference of mismatch rate (Diff) and fold change of mismatch rate (FC). Diff was calculated by subtracting the mismatch rate in the (+) demethylase from that

in the (−) demethylase sample, while FC was calculated by dividing the mismatch rate in the (−) demethylase by that in the (+) demethylase sample. FC was artificially set to “1000” if the mismatch rate in the (+) demethylase sample was “0”. A position was identified as an m^1A site when the following criteria were met: a) FC>=3; b) Diff>=10%; c) the number of reads with a mismatch at the position was no less than 5; d) criteria (a–c) were all fulfilled in both replicates.

In order to evaluate the frequency of potential false positives caused by m^1A-independent mismatch, we employed a reverse calling procedure. Specifically, the “reverse calculation” of Diff and FC values for each position were performed following the equations below:

$$\mathrm{Diff}_{\mathrm{opposite}}=(+)\mathrm{demethylase}-(-)\mathrm{demethylase};\mathrm{FC}_{\mathrm{opposite}}=(+)\mathrm{demethylase}/(-)\mathrm{demethylase}.$$

Under such circumstance, only 17 sites passed the above-mentioned threshold, suggesting the m^1A-independent mismatch should minimally interfere with the identification of true m^1A sites.

Identification of TRMT61B targets in mitochondrial-encoded transcripts—For the identification of TRMT61B targeting sites in mitochondrial-encoded RNA, the mismatch rate in the Input sample was firstly calculated for mock control sample and TRMT61B overexpression sample, respectively. Two parameters were defined to evaluate the increase of mismatch rate from the mock to TRMT61B o/e sample: difference of mismatch rate (Diff) and fold change of mismatch rate (FC). Diff was calculated by subtracting the mismatch rate in the mock sample from that in the TRMT61B o/e sample, while FC was calculated by dividing the mismatch rate in the TRMT61B o/e by that in the mock sample. FC was artificially set to “1000” if the mismatch rate in the mock sample was “0”. A position was identified as TRMT61B target when the following criteria were met: a) FC>=5; b) Diff>=5%; c) the site was covered by more than 500 sequencing reads; d) criteria (a–c) were all fulfilled in both replicates.

Motif discovery and GO enrichment analysis—For the analysis of sequence consensus, 15 nt of sequence neighboring each m^1A site was retrieved. These sequences were then subjected to DREME algorithm in MEME suite (Version 4.12.0) for the discovery of enriched motifs (Bailey et al., 2009). The shuffled input sequences were used as the background to eliminate potential false positives caused by the nucleotide composition.

Gene Ontology (GO) enrichment analyses were performed using DAVID web-based tool (http://david.abcc.ncifcrf.gov/) (Huang da et al., 2009).

Secondary structure and minimum free energy analysis—12 nucleotides of the 5′ end and 10 nucleotides of the 3′ end of each m^1A site (hence 23 nt sequence in total) were retrieved for local structure analysis. RNAfold (v2.3.4) (http://rna.tbi.univie.ac.at/cgi-bin/RNAfold.cgi) was used to predict the secondary structure and calculate the corresponding minimum free energy (MFE). The length of the loop where m^1A resides was determined based on the predicted structure; for an m^1A site that is not located in a loop, this value was

set to “0”. The significance test of MFE between m^1A sites within the GUUCRA motif and other m^1A sites was performed using Mann-Whitney U-test.

Ribosome profiling data analysis and TE calculation—Ribo-seq and corresponding RNA-seq reads were aligned to the transcriptome, and RPKM (Reads Per Kilobase per Million mapped reads) of each transcript was calculated. Translation efficiency (TE) was defined for each transcript as the ratio of the RPKM in Ribo-seq to the RPKM in RNA-seq.

For the analysis of influence of m^1A on mitochondrial gene translation, mitochondrial ribosome profiling data were downloaded from the GEO Datasets (GSE48933) (Rooijers et al., 2013). The depth of reads covered for each nucleotide along the mitochondrial transcripts was retrieved using Samtools depth tool.

miRNA target analysis—The predicted miRNA targeting sites on mitochondrial coding genes were downloaded from the miRWalk database (v2.0) (Dweep and Gretz, 2015), which depends on the base-paring between “seed region” and gene sequence. The minimum length required for the match of seed region was set to 7 nt. The experimentally identified miRNA targeting sites were retrieved from the published CLASH results (Helwak et al., 2013).

Detection of mitochondrial nascent protein synthesis—The TRMT61B knock-down cells and mock control cells were washed with pre-warmed methionine-free medium and incubated in methionine-free medium for 45 min. Then Cells were treated with 50 μg/mL emetine in methionine-free medium for 15 min to inhibit cytoplasmic protein synthesis. Further the medium was replaced with methionine-free medium containing 1mM methionine analog L-azidohomoalanine (AHA) (Click Chemistry Tools) and 50 μg/mL emetine. After incubation for 1 h, cells were harvested using clod PBS. Total proteins from different cell lines were quantified with the BCA protein assay kit (Thermo Fisher). Equal amount of AHA-containing proteins were labeled with Cy3 (Click Chemistry Tool) via Click Chemistry. The click reaction was performed in RIPA buffer containing 550 μM Cy3-alkyne, 4mM BTTAA-CuSO4 complex and 151.43mM sodium ascorbate. The reaction was incubated for 2 h at 25 °C with gentle vortex. The labeled proteins were purified by chloroform/methanol precipitation and separated in a 8%–16% gradient SDS-PAGE, and the SDS-PAGE gel was visualized by Typhoon 9500 scan. The gel was also subjected to coomassie blue staining as loading control.

Enrichment of nascent protein—The TRMT61B overexpression cell lines and mock control cell lines were washed with pre-warmed methionine-free medium and starved of methionine in the methionine-free medium for 1 h. Then the medium was replaced with methionine-free medium containing 1 mM L-azidohomoalanine (AHA). After incubation for 2 h, the cells were harvested using cold PBS. Equal amount of AHA-containing proteins were labeled by biotin-alkyne (Click Chemistry Tool) via click reaction. The purified proteins were incubated with 200 μL Streptavidin Agarose Resin (Thermo) in RIPA buffer for 3 h at 29 °C. Resins we re washed 3 times with PBS and 3 additional times with water. Proteins were reduced by incubated at 37 °C in the presence of 10mM DTT in 6M Urea in PBS for 30min and later alkylated by adding iodoacetamide (Sigma) to the final concentration of 20 mM for another 30min. Resins were sequentially washed once with PBS

and once with 100nM Triethylammonium bicarbonate (TEAB) buffer. Proteins were digested “on bead” with trypsin in 100 mM TEAB and 1 mM $CaCl_2$ buffer overnight at 37 °C. The peptide solution was performed reductive dimethylation labeling and analyzed on a Q Exactive mass spectrometer.

QUANTIFICATION AND STATISTICAL ANALYSIS

p-values were calculated using unpaired two-sided Mann-Whitney U-test. *$p < 0.05$, **$p < 0.01$. N.S. stands for not significant. Error bars represent mean ± SD.

DATA AND SOFTWARE AVAILABILITY

Sequencing data have been deposited into the Gene Expression Omnibus (GEO) under the accession number: GSE102040. Original imaging data have been deposited to Mendeley Data and are available at http://dx.doi.org/10.17632/bf8cshtzmx.1

ADDITIONAL RESOURCES

A detailed protocol describing m^1A-MAP used in this study is provided in Methods S1.

Supplementary Material

Refer to Web version on PubMed Central for supplementary material.

Acknowledgments

The authors would like to thank Prof. Ying Liu for advice on methyltransferase, Prof. Yongliang Zhao for sharing antibody, Prof. Xinxiang Zhang and Mr. Xiaohui Zhang for quantitative MS measurements, Prof. Xiaorong Zhang and Mr. Kuanxing Gao for metabolic labelling assay and the Core Facilities at the School of Life Sciences, Peking University. This work was supported by the National Basic Research Foundation of China (nos. 2016YFC0900301 and 2014CB964900 to C.Y.), the National Natural Science Foundation of China (nos. 21522201 and 91740112 to C.Y.), US National Institutes of Health (R01 AG042400 and R01 GM122814 to S.-B.Q) and HHMI Faculty Scholar (55108556 to S.-B.Q).

References

Anderson, JT., Droogmans, L. Biosynthesis and function of 1-methyladenosine in transfer RNA. In: Grosjean, H., editor. Fine-Tuning of RNA Functions by Modification and Editing. Berlin, Heidelberg: Springer Berlin Heidelberg; 2005. p. 121-139.

Antonicka H, Choquet K, Lin ZY, Gingras AC, Kleinman CL, Shoubridge EA. A pseudouridine synthase module is essential for mitochondrial protein synthesis and cell viability. Embo Rep. 2017; 18:28–38. [PubMed: 27974379]

Bailey TL, Boden M, Buske FA, Frith M, Grant CE, Clementi L, Ren J, Li WW, Noble WS. MEME SUITE: tools for motif discovery and searching. Nucleic Acids Res. 2009; 37:W202–208. [PubMed: 19458158]

Bar-Yaacov D, Frumkin I, Yashiro Y, Chujo T, Ishigami Y, Chemla Y, Blumberg A, Schlesinger O, Bieri P, Greber B, et al. Mitochondrial 16S rRNA Is Methylated by tRNA Methyltransferase TRMT61B in All Vertebrates. PLoS Biol. 2016; 14:e1002557. [PubMed: 27631568]

Bokar JA, Shambaugh ME, Polayes D, Matera AG, Rottman FM. Purification and cDNA cloning of the AdoMet-binding subunit of the human mRNA (N6-adenosine)-methyltransferase. RNA. 1997; 3:1233–1247. [PubMed: 9409616]

Carlile TM, Rojas-Duran MF, Zinshteyn B, Shin H, Bartoli KM, Gilbert WV. Pseudouridine profiling reveals regulated mRNA pseudouridylation in yeast and human cells. Nature. 2014; 515:143–146. [PubMed: 25192136]

Chujo T, Suzuki T. Trmt61B is a methyltransferase responsible for 1-methyladenosine at position 58 of human mitochondrial tRNAs. RNA. 2012; 18:2269–2276. [PubMed: 23097428]

Clark WC, Evans ME, Dominissini D, Zheng G, Pan T. tRNA base methylation identification and quantification via high-throughput sequencing. RNA. 2016; 22:1771–1784. [PubMed: 27613580]

Cozen AE, Quartley E, Holmes AD, Hrabeta-Robinson E, Phizicky EM, Lowe TM. ARM-seq: AlkB-facilitated RNA methylation sequencing reveals a complex landscape of modified tRNA fragments. Nat Methods. 2015; 12:879–884. [PubMed: 26237225]

Dominissini D, Nachtergaele S, Moshitch-Moshkovitz S, Peer E, Kol N, Ben-Haim MS, Dai Q, Di Segni A, Salmon-Divon M, Clark WC, et al. The dynamic N(1)-methyladenosine methylome in eukaryotic messenger RNA. Nature. 2016; 530:441–446. [PubMed: 26863196]

Dunn DB. The occurrence of 1-methyladenine in ribonucleic acid. Biochim Biophys Acta. 1961; 46:198–200. [PubMed: 13725042]

Dweep H, Gretz N. miRWalk2.0: a comprehensive atlas of microRNA-target interactions. Nat Methods. 2015; 12:697. [PubMed: 26226356]

Falkenberg M, Larsson NG, Gustafsson CM. DNA replication and transcription in mammalian mitochondria. Annu Rev Biochem. 2007; 76:679–699. [PubMed: 17408359]

Finer-Moore J, Czudnochowski N, O'Connell JD 3rd, Wang AL, Stroud RM. Crystal Structure of the Human tRNA m(1)A58 Methyltransferase-tRNA(3)(Lys) Complex: Refolding of Substrate tRNA Allows Access to the Methylation Target. J Mol Biol. 2015; 427:3862–3876. [PubMed: 26470919]

Frye M, Jaffrey SR, Pan T, Rechavi G, Suzuki T. RNA modifications: what have we learned and where are we headed? Nat Rev Genet. 2016; 17:365–372. [PubMed: 27140282]

Fu Y, Dominissini D, Rechavi G, He C. Gene expression regulation mediated through reversible m(6)A RNA methylation. Nat Rev Genet. 2014; 15:293–306. [PubMed: 24662220]

Hauenschild R, Tserovski L, Schmid K, Thuring K, Winz ML, Sharma S, Entian KD, Wacheul L, Lafontaine DL, Anderson J, et al. The reverse transcription signature of N-1-methyladenosine in RNA-Seq is sequence dependent. Nucleic Acids Res. 2015; 43:9950–9964. [PubMed: 26365242]

He C. Grand challenge commentary: RNA epigenetics? Nat Chem Biol. 2010; 6:863–865. [PubMed: 21079590]

Helm M, Motorin Y. Detecting RNA modifications in the epitranscriptome: predict and validate. Nat Rev Genet. 2017; 18:275–291. [PubMed: 28216634]

Helwak A, Kudla G, Dudnakova T, Tollervey D. Mapping the human miRNA interactome by CLASH reveals frequent noncanonical binding. Cell. 2013; 153:654–665. [PubMed: 23622248]

Huang da W, Sherman BT, Lempicki RA. Systematic and integrative analysis of large gene lists using DAVID bioinformatics resources. Nat Protoc. 2009; 4:44–57. [PubMed: 19131956]

Kondo A, Yamamoto S, Nakaki R, Shimamura T, Hamakubo T, Sakai J, Kodama T, Yoshida T, Aburatani H, Osawa T. Extracellular Acidic pH Activates the Sterol Regulatory Element-Binding Protein 2 to Promote Tumor Progression. Cell Rep. 2017; 18:2228–2242. [PubMed: 28249167]

Li H, Durbin R. Fast and accurate short read alignment with Burrows-Wheeler transform. Bioinformatics. 2009; 25:1754–1760. [PubMed: 19451168]

Li H, Handsaker B, Wysoker A, Fennell T, Ruan J, Homer N, Marth G, Abecasis G, Durbin R. Genome Project Data Processing S. The Sequence Alignment/Map format and SAMtools. Bioinformatics. 2009; 25:2078–2079. [PubMed: 19505943]

Li X, Xiong X, Wang K, Wang L, Shu X, Ma S, Yi C. Transcriptome-wide mapping reveals reversible and dynamic N(1)-methyladenosine methylome. Nat Chem Biol. 2016a; 12:311–316. [PubMed: 26863410]

Li X, Xiong X, Yi C. Epitranscriptome sequencing technologies: decoding RNA modifications. Nat Methods. 2016b; 14:23–31. [PubMed: 28032622]

Li X, Zhu P, Ma S, Song J, Bai J, Sun F, Yi C. Chemical pulldown reveals dynamic pseudouridylation of the mammalian transcriptome. Nat Chem Biol. 2015; 11:592–597. [PubMed: 26075521]

Liu F, Clark W, Luo G, Wang X, Fu Y, Wei J, Wang X, Hao Z, Dai Q, Zheng G, et al. ALKBH1-Mediated tRNA Demethylation Regulates Translation. Cell. 2016

Liu J, Yue Y, Han D, Wang X, Fu Y, Zhang L, Jia G, Yu M, Lu Z, Deng X, et al. A METTL3-METTL14 complex mediates mammalian nuclear RNA N6-adenosine methylation. Nat Chem Biol. 2014; 10:93–95. [PubMed: 24316715]

Lovejoy AF, Riordan DP, Brown PO. Transcriptome-wide mapping of pseudouridines: pseudouridine synthases modify specific mRNAs in S. cerevisiae. PLoS One. 2014; 9:e110799. [PubMed: 25353621]

Machnicka MA, Milanowska K, Osman Oglou O, Purta E, Kurkowska M, Olchowik A, Januszewski W, Kalinowski S, Dunin-Horkawicz S, Rother KM, et al. MODOMICS: a database of RNA modification pathways--2013 update. Nucleic Acids Res. 2013; 41:D262–267. [PubMed: 23118484]

Mauer J, Luo X, Blanjoie A, Jiao X, Grozhik AV, Patil DP, Linder B, Pickering BF, Vasseur JJ, Chen Q, et al. Reversible methylation of m6Am in the 5′ cap controls mRNA stability. Nature. 2017; 541:371–375. [PubMed: 28002401]

Mercer TR, Neph S, Dinger ME, Crawford J, Smith MA, Shearwood AM, Haugen E, Bracken CP, Rackham O, Stamatoyannopoulos JA, et al. The human mitochondrial transcriptome. Cell. 2011; 146:645–658. [PubMed: 21854988]

Ozanick S, Krecic A, Andersland J, Anderson JT. The bipartite structure of the tRNA m1A58 methyltransferase from S. cerevisiae is conserved in humans. RNA. 2005; 11:1281–1290. [PubMed: 16043508]

Ping XL, Sun BF, Wang L, Xiao W, Yang X, Wang WJ, Adhikari S, Shi Y, Lv Y, Chen YS, et al. Mammalian WTAP is a regulatory subunit of the RNA N6-methyladenosine methyltransferase. Cell Res. 2014; 24:177–189. [PubMed: 24407421]

Quiros PM, Prado MA, Zamboni N, D'Amico D, Williams RW, Finley D, Gygi SP, Auwerx J. Multi-omics analysis identifies ATF4 as a key regulator of the mitochondrial stress response in mammals. J Cell Biol. 2017; 216:2027–2045. [PubMed: 28566324]

Richter-Dennerlein R, Dennerlein S, Rehling P. Integrating mitochondrial translation into the cellular context. Nat Rev Mol Cell Biol. 2015; 16:586–592. [PubMed: 26535422]

Rooijers K, Loayza-Puch F, Nijtmans LG, Agami R. Ribosome profiling reveals features of normal and disease-associated mitochondrial translation. Nat Commun. 2013; 4:2886. [PubMed: 24301020]

Rorbach J, Minczuk M. The post-transcriptional life of mammalian mitochondrial RNA. Biochem J. 2012; 444:357–373. [PubMed: 22642575]

Roundtree IA, Evans ME, Pan T, He C. Dynamic RNA Modifications in Gene Expression Regulation. Cell. 2017; 169:1187–1200. [PubMed: 28622506]

Safra M, Nir R, Farouq D, Vainberg Slutskin I, Schwartz S. TRUB1 is the predominant pseudouridine synthase acting on mammalian mRNA via a predictable and conserved code. Genome Res. 2017; 27:393–406. [PubMed: 28073919]

Saikia M, Fu Y, Pavon-Eternod M, He C, Pan T. Genome-wide analysis of N1-methyl-adenosine modification in human tRNAs. RNA. 2010; 16:1317–1327. [PubMed: 20484468]

Saletore Y, Meyer K, Korlach J, Vilfan ID, Jaffrey S, Mason CE. The birth of the Epitranscriptome: deciphering the function of RNA modifications. Genome Biol. 2012; 13:175. [PubMed: 23113984]

Schwartz S, Bernstein DA, Mumbach MR, Jovanovic M, Herbst RH, Leon-Ricardo BX, Engreitz JM, Guttman M, Satija R, Lander ES, et al. Transcriptome-wide mapping reveals widespread dynamic-regulated pseudouridylation of ncRNA and mRNA. Cell. 2014a; 159:148–162. [PubMed: 25219674]

Schwartz S, Mumbach MR, Jovanovic M, Wang T, Maciag K, Bushkin GG, Mertins P, Ter-Ovanesyan D, Habib N, Cacchiarelli D, et al. Perturbation of m6A writers reveals two distinct classes of mRNA methylation at internal and 5′ sites. Cell Rep. 2014b; 8:284–296. [PubMed: 24981863]

Slomovic S, Laufer D, Geiger D, Schuster G. Polyadenylation and degradation of human mitochondrial RNA: the prokaryotic past leaves its mark. Mol Cell Biol. 2005; 25:6427–6435. [PubMed: 16024781]

Smits P, Smeitink J, van den Heuvel L. Mitochondrial translation and beyond: processes implicated in combined oxidative phosphorylation deficiencies. J Biomed Biotechnol. 2010; 2010:737385. [PubMed: 20396601]

Suzuki T, Nagao A, Suzuki T. Human mitochondrial tRNAs: biogenesis, function, structural aspects, and diseases. Annu Rev Genet. 2011; 45:299–329. [PubMed: 21910628]

Tabb DL, McDonald WH, Yates JR 3rd. DTASelect and Contrast: tools for assembling and comparing protein identifications from shotgun proteomics. J Proteome Res. 2002; 1:21–26. [PubMed: 12643522]

Temperley RJ, Wydro M, Lightowlers RN, Chrzanowska-Lightowlers ZM. Human mitochondrial mRNAs--like members of all families, similar but different. Biochim Biophys Acta. 2010; 1797:1081–1085. [PubMed: 20211597]

Van Nostrand EL, Pratt GA, Shishkin AA, Gelboin-Burkhart C, Fang MY, Sundararaman B, Blue SM, Nguyen TB, Surka C, Elkins K, et al. Robust transcriptome-wide discovery of RNA-binding protein binding sites with enhanced CLIP (eCLIP). Nat Methods. 2016; 13:508–514. [PubMed: 27018577]

Vilardo E, Nachbagauer C, Buzet A, Taschner A, Holzmann J, Rossmanith W. A subcomplex of human mitochondrial RNase P is a bifunctional methyltransferase--extensive moonlighting in mitochondrial tRNA biogenesis. Nucleic Acids Res. 2012; 40:11583–11593. [PubMed: 23042678]

Waku T, Nakajima Y, Yokoyama W, Nomura N, Kako K, Kobayashi A, Shimizu T, Fukamizu A. NML-mediated rRNA base methylation links ribosomal subunit formation to cell proliferation in a p53-dependent manner. J Cell Sci. 2016; 129:2382–2393. [PubMed: 27149924]

Weerapana E, Wang C, Simon GM, Richter F, Khare S, Dillon MB, Bachovchin DA, Mowen K, Baker D, Cravatt BF. Quantitative reactivity profiling predicts functional cysteines in proteomes. Nature. 2010; 468:790–795. [PubMed: 21085121]

Xu T, Park SK, Venable JD, Wohlschlegel JA, Diedrich JK, Cociorva D, Lu B, Liao L, Hewel J, Han X, et al. ProLuCID: An improved SEQUEST-like algorithm with enhanced sensitivity and specificity. J Proteomics. 2015; 129:16–24. [PubMed: 26171723]

You C, Dai X, Wang Y. Position-dependent effects of regioisomeric methylated adenine and guanine ribonucleosides on translation. Nucleic Acids Res. 2017

Zhang X, Zuo X, Yang B, Li Z, Xue Y, Zhou Y, Huang J, Zhao X, Zhou J, Yan Y, et al. MicroRNA directly enhances mitochondrial translation during muscle differentiation. Cell. 2014; 158:607–619. [PubMed: 25083871]

Zheng G, Qin Y, Clark WC, Dai Q, Yi C, He C, Lambowitz AM, Pan T. Efficient and quantitative high-throughput tRNA sequencing. Nat Methods. 2015; 12:835–837. [PubMed: 26214130]

Zubradt M, Gupta P, Persad S, Lambowitz AM, Weissman JS, Rouskin S. DMS-MaPseq for genome-wide or targeted RNA structure probing in vivo. Nat Methods. 2017; 14:75–82. [PubMed: 27819661]

Highlights

1. We report "m^1A-MAP", a misincorporation-based method, to map m^1A at base resolution
2. m^1A-MAP detects m^1A methylation at mRNA cap and 5′-UTR
3. m^1A-MAP reveals prevalent m^1A modification in mitochondrial-encoded transcripts
4. m^1A in different mRNA regions differentially impacts translation

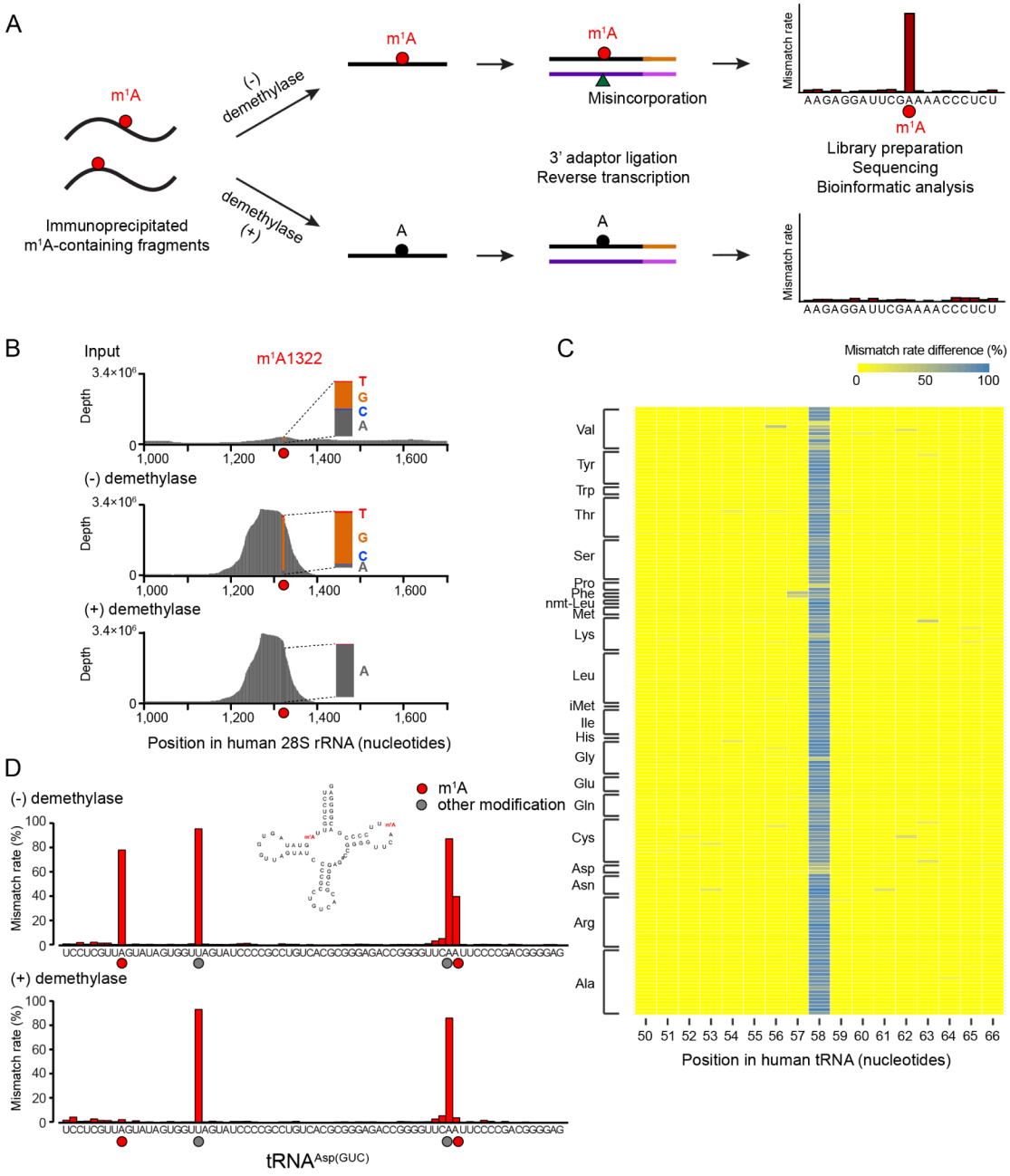

Figure 1. m^{1}A-MAP utilizes m^{1}A-induced misincorporation to detect m^{1}A sites at single-nucleotide resolution

(**A**) Scheme of m^{1}A-MAP. We optimized the conditions of RT so as to allow efficient misincorporation in cDNA synthesis. The use of an m^{1}A antibody pre-enriches the m^{1}A-containing RNA fragments, thereby maximizing the misincorporation signal; and the use of demethylase treatment improves the confidence of detection. An m^{1}A modification is called depending on the difference and fold change of mismatch rate between the (−) and (+) demethylase samples (see Method Details).

(**B**) m^{1}A-MAP maximizes the misincorporation signal for m^{1}A1322 on 28S rRNA.

(**C**) m^1A-MAP detects m^1A58 for the cytosolic tRNAs. Shown here is the difference of mismatch rate between the (−) and (+) demethylase samples.
(**D**) m^1A-MAP detects an m^1A site at position 9 in the cytosolic human $tRNA^{Asp(GUC)}$. The mismatch rate for m^1A58 is also reduced after demethylase treatment, while two other modifications (at position 20 and 57) are not sensitive to demethylation, representing other types of RNA modifications.
See also Figure S1 and S2.

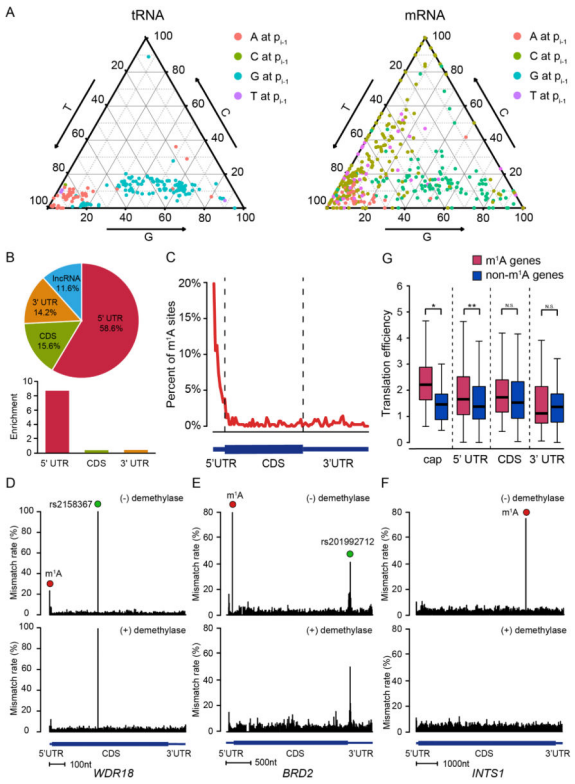

Figure 2. Single-nucleotide resolution m^{1}A methylome in the human transcriptome

(**A**) Mutation pattern of m^{1}A sites in mRNA resembles that in tRNA. Shown here is the sequence-dependent mutation profile of m^{1}A sites with regard to the immediate 5′ nucleotide.

(**B**) The pie chart shows the percentage of m^{1}A sites in each non-overlapping segment.

(**C**) Distribution of m^{1}A sites across mRNA segments. Each segment was normalized according to its average length in Refseq annotation.

(**D–F**) Representative views of a typical m^{1}A site at the cap+1 position (the first transcribed nucleotide of mRNA) of *WDR18* (**D**), the 5′-UTR of *BRD2* (**E**), and the CDS of *INTS1* mRNA (**F**). The demethylation-insensitive signals in (**D**) and (**E**), which are indicated as green dots, are known SNPs. The scale bars are indicated at the bottom of each panel.

(**G**) m^{1}A in the cap (24 sites at the cap+1 and 3 sites at the cap+2 position) and 5′-UTR positively correlates with increased translation efficiency. Transcripts with comparable expression level but without m^{1}A sites were chosen as the negative control for each category.

See also Figure S3.

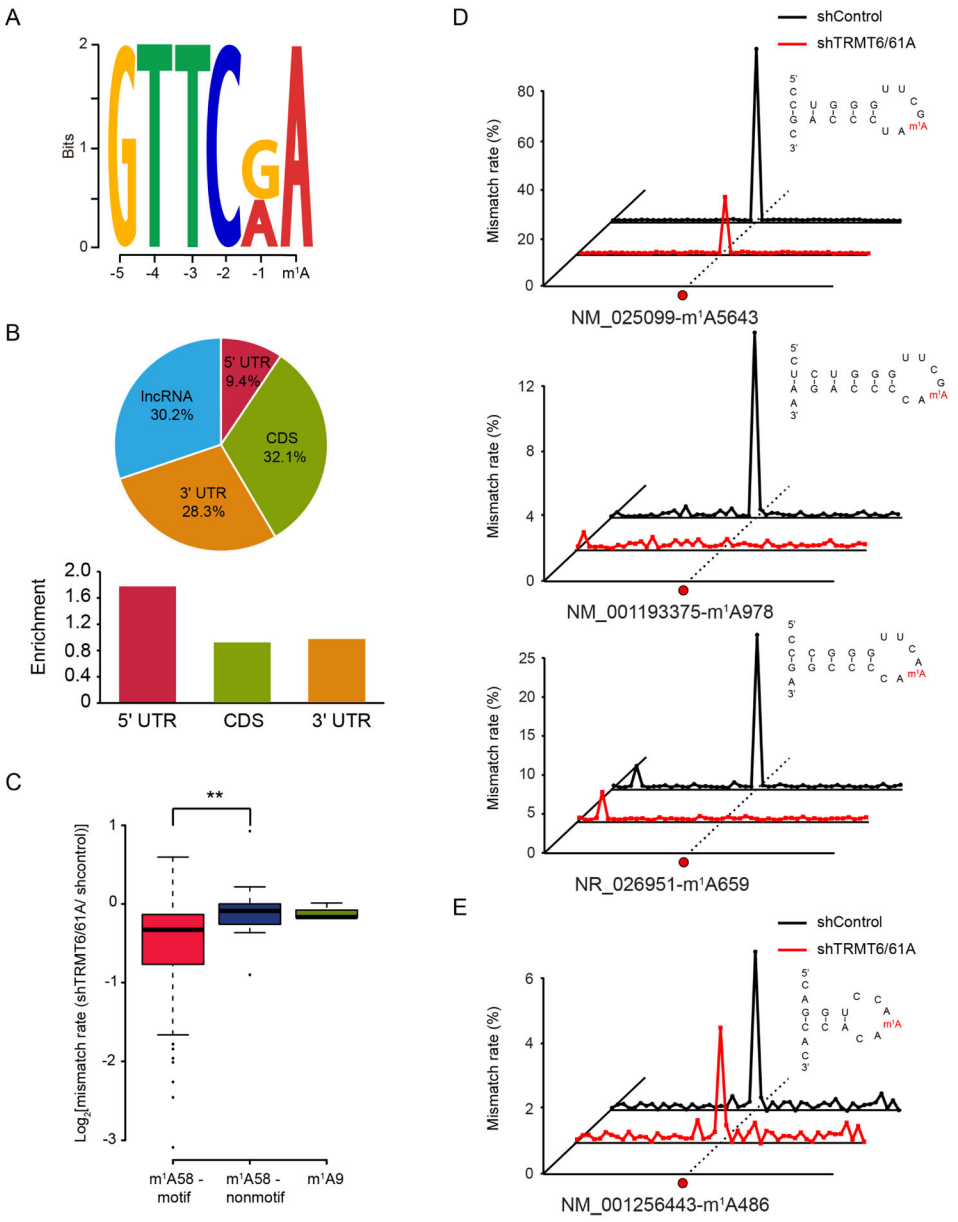

Figure 3. The tRNA methyltransferase complex TRMT6/61A catalyzes a subset of m1A methylation in mRNA

(**A**) Motif analysis revealed a GUUCRA tRNA-like consensus for a group of m^1A in mRNA, E-value=4.8e-009.

(**B**) Pie chart showing the percentage of m^1A sites in each non-overlapping segment. Comparing to the non-motif m^1A sites in mRNA, these sites are evenly distributed in the transcriptome.

(**C**) TRMT6/61A specifically targets m^1A within the consensus sequence, while doesn't work on m^1A in non-motif sequence of the T-loop nor m^1A at the 9th position of tRNA, p-value <0.005.

(**D**) Representative views of three mRNA targets of TRMT6/61A. The predicted RNA secondary structures are also shown, revealing a conserved stem-loop structure that harbors the GUUCRA motif.

(**E**) An example of non-motif mRNA m^1A site, showing similar mismatch rates in the control and TRMT6/61A knock-down samples.

See also Figure S4.

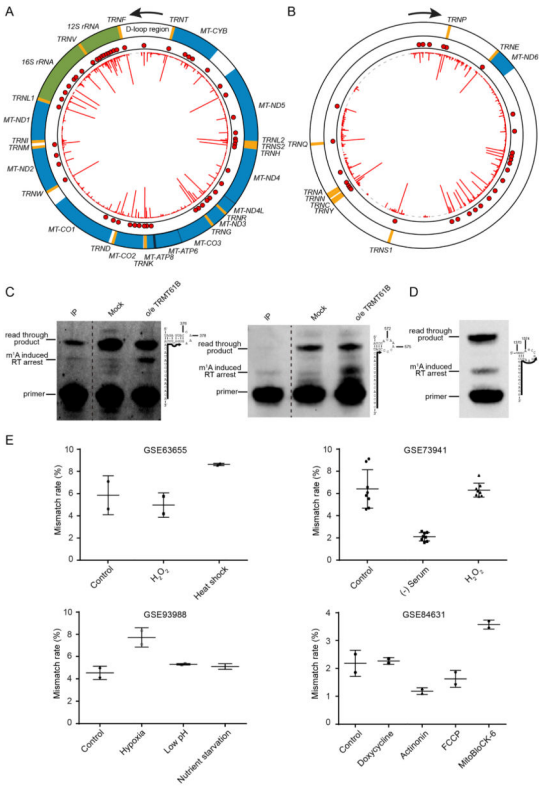

Figure 4. Distinct m^{1}A methylome in the mitochondrial transcriptome

(**A**) m^{1}A methylome of the heavy strand. Orange, green and blue colors represent tRNA, rRNA and mRNA, respectively. The red line in the inner circle represents the difference of mismatch rate of individual nucleotide while each red dot represents an identified m^{1}A site.

(**B**) m^{1}A methylome of the light strand.

(**C**) Detection of two novel m^{1}A sites at position 378 and 575 in 12S mt-rRNA using a primer extension assay. In the immunoprecipitated samples (denoted as “IP”), the m^{1}A modification at the two sites can be unambiguously detected. In the mock control samples (without immunoprecipitation), the bands corresponding to m^{1}A378 and m^{1}A575 induced reverse transcription (RT) arrest were weak, indicating a relatively low stoichiometry of these sites. Upon TRMT61B overexpression, strong bands were observed, suggesting that these two sites can be targeted by TRMT61B. The primers are shown as solid lines next to the RNA sequence.

(**D**) Detection of m^{1}A1374 in *MT-ND5* mt-mRNA using the primer extension assay. A strong band that corresponds to m^{1}A1374 induced RT arrest can be found in the wild-type sample without immunoprecipitation, indicating a high modification level of this site. The primer is shown as solid lines next to the RNA sequence.

(**E**) m^{1}A1374 in *MT-ND5* is dynamically regulated by different stress conditions. Mismatch signal of m^{1}A1374 could be consistently detected in multiple publicly available RNA-seq data and is regulated upon environmental stress.

See also Figure S5.

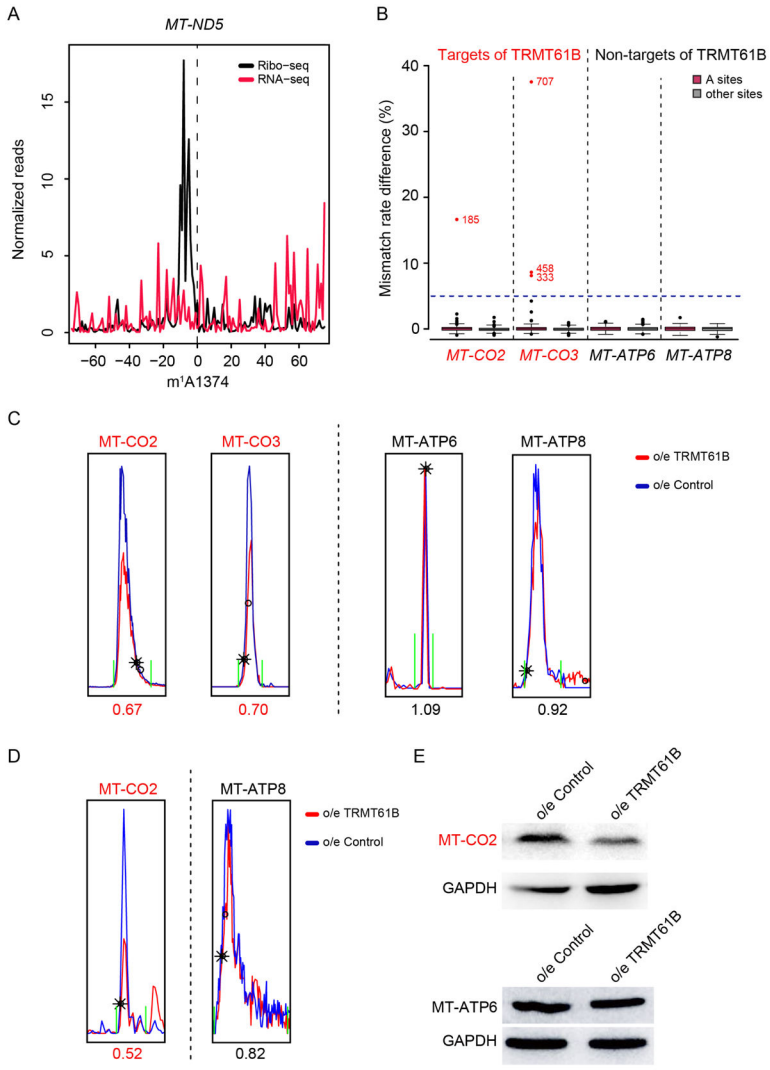

Figure 5. m^{1}A in the mitochondrial mRNA interferes with translation

(**A**) Mitochondrial ribosome stalling at the m^{1}A site of the *MT-ND5* mRNA. The density of the 5′ end of footprints was calculated for each position surrounding the m^{1}A site. Ribosome profiling and RNA-seq data was taken from a published study (see Method Details).

(**B**) TRMT61B overexpression greatly increased the m^{1}A modification level for several sites in *MT-CO2* and *MT-CO3*, while the modification status of *MT-ATP6 and MT-ATP8* remained unchanged. The red dots represent the targets of TRMT61B in *MT-CO2* and *MT-CO3*.

(**C**) Extracted ion chromatograms of MT-CO2 and MT-CO3 (two targets of TRMT61B) showed decreased protein level upon TRMT61B overexpression, while those of MT-ATP8 and MT-ATP6 (non-targets of TRMT61B) remained unchanged.

(**D**) Extracted ion chromatograms of nascent MT-CO2 and MT-ATP8 upon TRMT61B overexpression. The nascent protein level of MT-CO2 decreased while that of MT-ATP8 remained unaffected.

(**E**) Western blot of MT-CO2 and MT-ATP6 upon TRMT61B overexpression. See also Figure S5.